Research Square

Preprints are preliminary reports that have not undergone peer review.
They should not be considered conclusive, used to inform clinical practice,
or referenced by the media as validated information.

FveMYB117a and SL1 cooperatively regulate leaf morphogenesis in woodland strawberry

Yafan Han
Hebei Academy of Agriculture and Forestry Sciences, Shijiazhuang Fruit Tree Research Institute
Jia Feng
Hebei Academy of Agriculture and Forestry Sciences, Shijiazhuang Fruit Tree Research Institute
Peng Lu
Hebei Academy of Agriculture and Forestry Sciences, Shijiazhuang Fruit Tree Research Institute
Li Li
Hebei Academy of Agriculture and Forestry Sciences, Shijiazhuang Fruit Tree Research Institute
Mengjia Yang
Hebei Academy of Agriculture and Forestry Sciences, Institute of Agricultural Information and Economics
Lei Yang
Hebei Academy of Agriculture and Forestry Sciences, Shijiazhuang Fruit Tree Research Institute
Chunying Kang
ckang@mail.hzau.edu.cn

College of Horticulture and Forestry, Huazhong Agricultural University

Research Article

Keywords: strawberry, leaf development, FveMYB117a, SL1, auxin, cytokinin

Posted Date: October 9th, 2026

DOI: https://doi.org/10.21203/rs.3.rs-10948482/v1

License: This work is licensed under a Creative Commons Attribution 4.0 International License.
Read Full License

Additional Declarations: No competing interests reported.

Abstract

Background

Leaves function as the primary photosynthetic organs that produce energy for plant growth and development. In strawberries (*Fragaria* L.), mature leaves are trifoliate with serrated margins. Both *FveMYB117a* and *SL1* (*SIMPLE LEAF1*) play crucial roles in regulating strawberry leaf development. Nevertheless, the genetic relationship between these two genes and their underlying molecular regulatory mechanisms remain uncharacterized.

Results

The *fvemyb117a* mutant produces leaves with 1–5 leaflets, while the *sl1* mutant predominantly forms single-leaflet leaves. The *fvemyb117a sl1* double mutant produces only one small leaflet, with both the number of serrations and leaf area significantly reduced. Several lines of evidence demonstrate that FveMYB117a indirectly activates *SL1* expression in leaves. Transcriptome analysis shows that a number of transcription factors and genes involved in the auxin and cytokinin pathways are downregulated in all three mutants. In young leaves, auxin levels are significantly lower in the mutants than the wild-type control; cytokinin levels are markedly elevated in *fvemyb117a*, but significantly reduced in both *sl1* and the *fvemyb117a sl1* double mutant.

Conclusions

These results indicate that *SL1* is epistatic to *FveMYB117a* in leaflet initiation, whereas the two genes exert additive effects on leaf serration formation. Together, they constitute an interactive regulatory network that coordinately modulates leaf morphogenesis in woodland strawberry.

Background

As pivotal vegetative organs, leaves host a wealth of essential physiological processes, including photosynthesis, transpiration, and gas exchange. Leaf morphology exhibits remarkable diversity among plant taxa, with diverse traits such as distinct leaf size and shape [1]. In compound-leafed species, leaf primordia are first initiated on the flanks of the shoot apical meristem (SAM), followed by the formation of leaflet primordia and marginal serrations, and ultimately by three-dimensional expansion of the leaf blade [2–4]. To date, the molecular mechanisms orchestrating leaf development have been extensively elucidated in model plants such as *Arabidopsis thaliana*, tomato, and *Medicago*. Strawberry produces compound leaves with a stereotyped developmental sequence. Investigations into strawberry leaf morphogenesis will greatly advance our understanding of conserved and species-specific genetic regulatory networks when combined with findings from other plant species.

Recent studies have established that leaf development is orchestrated by a diverse array of transcription factors acting at multiple regulatory levels. The Class I *KNOTTED1-LIKE HOMEOBOX* (*KNOXI*) genes are well-established as critical positive regulators of leaf complexity [5–9]. In *Cardamine hirsuta*, the transcription factor *RCO* (*REDUCED COMPLEXITY*) is primarily responsible for the divergence in leaf morphology between this species and Arabidopsis [10]. The *CIN-TCP* transcription factors negatively regulate the expression of *CUC* genes by activating *miR164* and *AS1* (*ASYMMETRIC LEAVES1*) [11–14]. The *WOX* genes play critical roles in the regulation of leaf width [15–17]. Loss-of-function mutations in the zinc-finger transcription factor gene *JAG* lead to distinct leaf shape phenotypes across species: serrated margins in Arabidopsis [18], diminished compound leaf complexity in tomato [19], and narrowed leaflets in *soybean* [20]. In pea and *Medicago*, compound leaf patterning is controlled by *UNIFOLIATA* (*UNI*) and *SINGLE LEAFLET1* (*SGL1*), two orthologs of the well characterized floral meristem identity gene *LEAFY* (*LFY*) [21–22]. In *Medicago*, the C2H2-type transcription factor PALM1, BEL1-like domain-containing PINNA1, and the GRAS-family PINNA2 collectively repress leaflet formation by directly inhibiting *SGL1* expression [23–25].

Auxin and cytokinin serve as two major hormonal regulators of leaf development, generally exerting promotive effects. Local auxin accumulation is essential for the initiation of leaflet and serration primordia, establishing auxin maxima at the tips of emerging leaflets or along the margins of leaf serrations [3, 26–27]. Multiple studies have demonstrated that mutations in auxin-pathway-related genes alter leaf shape. Mutation in the auxin-biosynthesis gene *YUC* impairs normal initiation of lateral leaflets in *Medicago* [28]. Loss-of-function mutations in the auxin efflux carrier gene *PIN1* convert the compound leaves of *Cardamine hirsuta* into simple ones [29–30]. In tomato, both reduced expression of *SlIAA9* and a single-nucleotide deletion within this gene cause simplified leaf morphology [31–32]. Cytokinins also modulate leaf morphological complexity. Ectopic expression of the cytokinin-biosynthesis gene *AtIPT7* in tomato significantly increases leaflet number, whereas overexpression of the cytokinin-catabolic gene *AtCKX3* yields the opposite phenotype [33]. Exogenous cytokinin application triggers supernumerary leaflet formation and enhances serration depth along leaf margins [34–35]. The final leaf morphology is determined by synergistic and antagonistic crosstalk between auxin and cytokinin.

Strawberries normally produce trifoliate leaves, comprising a single terminal leaflet and two lateral leaflets. In woodland strawberry, mutations in *FveLFYa* cause a small proportion of leaves to exhibit smaller leaflets, or, in severe cases, result in a reduction of leaflet number from three to two [36]. *SALAD* encodes single-MYB domain transcription factor that regulates both leaf serration depth and leaf area [37]. *FvemiR164a* is involved in the regulation of leaf serration, and allelic mutants of its target gene *FveCUC2a* exhibit smooth leaf margins and fused leaflets [38]. Mutations in *FvePHP*, which encodes a DNA-polymerase-related protein, lead to markedly reduced serrations and decreased leaf area [39]. The histone methylation complex gene *ULTRAPETALA1* (*ULT1*) positively regulates leaf complexity; its disruption not only leads to the formation of 4–5 leaflets in roughly 30% of mature leaves but also significantly enhances leaf width and area [40]. The KNOX family members in woodland strawberry are resolved into three distinct evolutionary lineages (*FveKNOXI*, *FveKNOXII* and *FveKNOXM*) [37]. The Class I clade comprised *FveSTMa*, *FveSTMb*, *FveBP*, *FveKNOX1*, *FveKNAT2/6La* and *FveKNAT2/6Lb*. By contrast,

Class II was defined by *FveKNAT7*, *FveKNAT5La* and *FveKNAT5Lb*. The remaining members, *FveKNOXMa* and *FveKNOXMb*, clustered independently as the KNATM subclass. Downregulation of *FaKNOX1* expression in cultivated strawberries (*Fragaria* × *ananassa*) results in elongated rachis and deeper serrations, whereas serration and leaflet numbers remain unchanged [41]. These findings demonstrate that leaf shape morphogenesis in strawberry is under polygenic control.

Previously, we revealed that FveMYB117a controls leaf morphology by directly regulating the expression levels of the auxin biosynthesis gene *FveYUC4*, the cytokinin biosynthesis gene *FveIPT2*, the cytokinin degradation gene *FveCKX1*, and *FveCUC2a* [42]. The *simple leaf 1* (*sl1*) and the natural *monophyla* mutant are allelic; both exhibit a single leaflet per petiole, and their phenotypes result from mutations in a gene encoding a transcription factor with a DNA-binding GT-1 domain and a protein kinase PKc domain [43]. However, the genetic relationship and molecular mechanism between *FveMYB117a* and *SL1* during leaf development remain largely unknown. To address this, we generated and characterized the *fvemyb117a-1 sl1-1* double mutant to dissect their genetic and molecular interactions, identified their co-regulated target genes, and assessed their combined effects on auxin and cytokinin metabolism. Our findings provide new insights into the complex regulatory network underlying leaf development, offering valuable gene resources as well as a theoretical basis for molecular breeding tailored to optimize strawberry leaf morphology.

Results

FveMYB17a acts synergistically with *SL1* during leaf development

Prior studies showed that the *fvemyb117a-1* mutant produces 1 to 5 leaflets per leaf at random, accompanied by reduced numbers of leaf serrations and leaf size [42]. Loss of *SL1* function impairs lateral leaflet primordium formation, predominantly yielding simple leaves and significantly decreasing leaf area [43]. To investigate the genetic interaction between *FveMYB117a* and *SL1* during leaf morphogenesis, we generated the *fvemyb117a-1 sl1-1* double mutant by crossing the respective single mutants. The results showed that in wild-type (WT) plants, 100% of the leaves were trifoliate; in *fvemyb117a-1*, leaves with 1 to 2 leaflets accounted for 24.75%, leaves with 3 leaflets accounted for 51.49%, and leaves with 4 to 5 leaflets accounted for 23.76%; in *sl1-1*, leaves with 1 to 2 leaflets accounted for 100% (96.83% were single leaves, 3.17% had 2 leaflets); whereas all the leaves in *fvemyb117a-1 sl1-1* were simple (Fig. 1A and 1B). This shows that *sl1-1* is epistatic to *fvemyb117a-1* in the regulation of leaflet primordium initiation.

To further delineate the shape characteristics of the leaves, we initially analyzed their overall outlines by calculating the leaf shape index (length/width), which was 1.47, 1.75, 1.18, and 1.82 for WT, *fvemyb117a-1*, *sl1-1*, and *fvemyb117a-1 sl1-1*, respectively (Fig. 1C). We subsequently assessed the leaf area, which measured 12.98 cm², 7.83 cm², 10.64 cm², and 2.53 cm² across the four genotypes (Fig. 1D). Finally, a more detailed analysis of marginal serrations yielded average counts of 14.75, 8.1, 14.25, and 4.45, respectively (Fig. 1E). Compared with either single mutant, the *fvemyb117a-1 sl1-1* double mutant

exhibited significantly reduced leaf area and fewer serrations, suggesting that *FveMYB117a* and *SL1* act synergistically to regulate leaf development in strawberry.

In addition, the double mutant *fvemyb117a-1 sl1-1* not only displayed a markedly distinct leaf morphology compared to WT but also exhibited significantly shortened petioles (Fig. 1F). Quantitative analysis of petiole length revealed that the *fvemyb117a-1* single mutant did not differ significantly from the WT, whereas the *sl1-1*single mutant showed a 24.70% reduction, and notably, the double mutant exhibited a drastic decrease of 77.51% (Fig. 1G). Collectively, these results suggest that *FveMYB117a* and *SL1* function synergistically to positively regulate petiole elongation in woodland strawberry.

FveMYB117a indirectly promoted the expression of *SL1*

Transcriptome analysis of the *fvemyb117a-1* young leaves identified that *SL1* is significantly downregulated (Fig. 2A) [42]. To validate this result, we examined *SL1* expression in young leaves of WT, *fvemyb117a-1*, and two independent complementation lines (*Comp*-L1 and *Comp*-L2). We found that *SL1* expression levels were significantly reduced in *fvemyb117a-1* and increased in the *FveMYB117a* complementation lines (Fig. 2B). Since the expression levels of *SL1* are opposite in *fvemyb117a-1* and its complementation lines, and given the phenotypic observations, we propose that *SL1* may function as a downstream target of *FveMYB117a* in the regulation of leaf development.

R2R3-MYB transcription factors can directly bind to the ACC(A/T)A(A/C)(T/C) *cis*-regulatory elements [45]. To determine whether FveMYB117a directly binds to the *SL1* promoter, we analyzed its promoter sequence. The results show that there is one prominent binding site (P1-ACCAACC) in the *SL1* promoter (Fig. 2C). First, we performed a yeast one hybrid (Y1H) assay to test the binding capacity. The results showed that FveMYB117a can interact with the P1 fragment in the *SL1* promoter (Fig. 2D). To test whether FveMYB117a affects the expression level of *SL1*, a dual luciferase (LUC) assay was then performed in *Nicotiana benthamiana* leaves using FveMYB117a as the effector and LUC driven by the *SL1* promoter (2 kb, including the P1 fragment) as the reporter. Compared to *p*35S (empty vector), the LUC signals of *pSL1*:*LUC* were significantly increased by *p35S*:*FveMYB117a* (Fig. 2E), suggesting that FveMYB117a activates the expression of *SL1*. However, in the electrophoretic mobility shift assay (EMSA), incubation of the purified recombinant FveMYB117a-His protein with the predicted target sequence within the *SL1* promoter P1 fragment failed to yield any detectable DNA-protein complex. These results suggest that FveMYB117a may indirectly activate *SL1* expression.

Identification of genes co-regulated by FveMYB117a and SL1 using RNA-seq

To identify genes co-regulated by *FveMYB117a* and *SL1*, we performed transcriptome analysis on the young leaves (SAM and up to P4 leaves) of both WT, *fvemyb117a-1*, *sl1-1*, and *fvemyb117a-1 sl1-1* with three biological replicates (Fig. S1). Each library yielded between 41.9 and 52.4 million reads, with an average mapping percentage of 98.68% to the woodland strawberry V4 genome (Supplementary Table S1). Principal Component Analysis (PCA) reveals that the three biological replicates for each genotype form tight, distinct clusters, whereas the replicates from the four different genotypes are clearly

separated from one another (Fig. 3A). This clear partitioning confirms the high reliability of the transcriptome dataset and validates its suitability for gene expression analyses. Pairwise comparisons against WT identified 1,250, 2,366, and 3,559 significantly upregulated genes in *fvemyb117a-1*, *sl1-1*, and *fvemyb117a-1 sl1-1*, respectively, along with 1,906, 2,867, and 3,316 significantly downregulated genes (fold change > 1.5, $P < 0.05$) (Fig. 3B, Supplementary Data Set 1-Set 3). The downregulated genes are enriched in various KEGG terms, such as plant hormone signal transduction and MAPK signaling pathway (Fig. S2-S4, Supplementary Data Set 4-6). We identified 754 commonly upregulated genes and 1,192 commonly downregulated genes across all three mutants (Fig. 3C and 3D, Supplementary Data Set 7). These genes are potential downstream genes jointly regulated by *FveMYB117a* and *SL1* in woodland strawberry leaf development.

A total of 1,451 transcription factors have been identified in woodland strawberry genome [46]. Given their regulatory significance, we systematically analyzed the transcription factors present in the co-regulated gene sets. Specifically, among the concurrently upregulated genes, 58 were transcription factors (Fig. S5A), predominantly belonging to the AP2/ERF-ERF, MYB, bHLH, HB-KNOX, and GARP-G2-like families (Fig. S5C). Among the downregulated genes, 109 were transcription factors (Fig. S5B), which mainly comprised the MYB, NAC, AP2/ERF-ERF, WRKY, and C2H2 families Fig. S5D).

FveMYB117a and SL1 cooperatively regulate transcription factor expression during leaf development.

Heatmap and RT-qPCR data consistently showed that *SL1* was significantly downregulated in *fvemyb117a-1*, *sl1-1*, and *fvemyb117a-1 sl1-1*; notably, *fvemyb117a-1 sl1-1* displayed a stronger reduction in *SL1* expression relative to either single mutant (Fig. 4A and 4B). As multiple transcription factors have been implicated in the regulation of leaf development across Arabidopsis, *Medicago* and tomato, we first investigated the transcription factors among the commonly downregulated genes. In the double mutants, the expression levels (TPM) of *FveKNAT5La*, *FveTCP4*, *FveTCP14*, *FveWOX1*, and *FveJAG* were each lower than the corresponding values observed in any of the single mutants (Fig. 4A). To validate these findings, their expression levels were quantified by RT-qPCR in young leaves collected from WT, *fvemyb117a-1*, *sl1-1*, and *fvemyb117a-1 sl1-1*. We found that *FveKNAT5La* expression was downregulated in the *fvemyb117a-1* mutant, with a more pronounced reduction in *sl1-1* and *fvemyb117a-1 sl1-1*; however, no significant difference was observed between the latter two genotypes (Fig. 4C). The *FveTCP4* transcript levels were similarly reduced in *fvemyb117a-1* and *sl1-1*, with the most substantial decrease occurring in *fvemyb117a-1 sl1-1* (Fig. 4D). Additionally, *FveTCP14*, *FveWOX1*, and *FveJAG* displayed a stepwise decreasing expression pattern across all three mutants (Fig. 4E-4G). These results show that FveMYB117a and SL1 can modulate the expression levels of *FveKNAT5La*, *FveTCP4*, *FveTCP14*, *FveWOX1*, and *FveJAG*, which potentially participate in the regulation of leaf morphology.

FveMYB117a and SL1 coordinate auxin and cytokinin pathways during leaf development

FveMYB117a and SL1 have been shown to regulate leaf shape development via auxin and cytokinin signaling pathways [42,43]. We thus focused on the differentially expressed genes (DEGs) associated with auxin and cytokinin pathways that were commonly downregulated across all three mutant

backgrounds. Heatmap shows that the transcript levels of the auxin biosynthesis genes (*FveYUC7* and *FveYUC6*), the auxin metabolism genes (*FveGH3.6* and *FveGH3.2*), and the cytokinin biosynthesis gene (*FveLOG8*) were markedly lower in the *fvemyb117a-1 sl1-1* double mutant than in the WT and the two corresponding single mutants (Fig. 5A). Given that the TPM values for *FveYUC7* remained below 1.0 across all four genotypes, its contribution to leaf development is likely negligible. Accordingly, RT-qPCR was employed to examine the expression profiles of the remaining four genes. The results revealed that *FveYUC6* and *FveGH3.6* were also downregulated in the single mutants, with a more pronounced reduction in *sl1-1* and the strongest suppression observed in the double mutant (Fig. 5B and 5C). *FveGH3.2* exhibited similar downregulation levels in both single mutants, while the double mutant displayed the most substantial decrease (Fig. 5D). As for *FveLOG8*, its expression was reduced in both single mutants-particularly in *fvemyb117a-1*, and reached its lowest level in the double mutant (Fig. 5E).

To investigate the involvement of auxin and cytokinin in leaf development regulated by *FveMYB117a* and *SL1*, young leaves (SAM and up to P4 leaves) were collected to quantify the endogenous hormone contents. Relative to the WT, free IAA and OX-IAA levels showed a progressive decrease across the *fvemyb117a-1*, *sl1-1*, and *fvemyb117a-1 sl1-1* (Fig. 6A and 6B). The isoprenoid cytokinins (CKs) detected in plants comprise four distinct molecular species: isopentenyladenine (iP), trans-zeatin (tZ), cis-zeatin (cZ), and dihydrozeatin (DZ) [47]. These compounds were significantly upregulated in *fvemyb117a-1* but downregulated in *sl1-1* and *fvemyb117a-1 sl1-1*, with the decrease in the double mutant exceeding that in *sl1-1* (Fig. 6C-6F). Collectively, these results demonstrate that FveMYB117a and SL1 cooperatively regulate leaf development, likely by modulating auxin and cytokinin levels.

Discussion

Leaves serve as the primary sites of photosynthesis in plants, exhibiting considerable diversity in both morphology and architecture. Strawberry, a globally cultivated fruit crop belonging to the Rosaceae family, possesses leaves with characteristic trifoliate organization and serrated margins. In this study, we found that *SL1* exhibits genetic epistasis over *FveMYB117a* during leaf primordium initiation, and FveMYB117a indirectly activates the expression of *SL1*. Furthermore, our results demonstrate that FveMYB117a and SL1 coordinately modulate leaf development by orchestrating the expression of multiple transcription factors, as well as genes involved in auxin and cytokinin signaling pathways, and by concomitantly influencing endogenous hormone levels.

FveMYB117a indirectly activates *SL1* to synergistically regulate leaf development

The biological functions of FveMYB117a orthologs have been extensively investigated in Arabidopsis and tomato. In Arabidopsis, the *lof1* mutant leaves display no discernible phenotypic alterations [53]. However, in tomato the *tf* mutant consistently produces fewer leaflets than the wild type, a phenotype attributed to reduced morphogenetic competence at the leaf margin [54-55]. Moreover, the orthologs of SL1, AGLF (*Medicago*) and SlGT11 (tomato) exert only minor effects on leaf development [56-58]. In striking contrast, mutations in *FveMYB117a* and *SL1* in woodland strawberry result in diverse leaf

phenotypes, including altered numbers of leaf primordia, decreased leaf area, and fewer marginal notches (Fig. 1). These observations indicate that FveMYB117a and SL1 function differently from their homologs in Arabidopsis and tomato, suggesting that this functional divergence may be associated with the evolutionary trajectory of these genes.

Mechanistically, SL1 acts upstream to indirectly activate *FveLFYa* expression within the regulatory framework governing leaf development [43]. At the early stage (P2), SL1 positively regulates *FveCUC2a* expression to promote leaflet separation, while at the later stage (P3), SALAD negatively regulates *FveCUC2a* to limit the depth of serrations, thus finely coordinating the establishment of leaf margin complexity [37]. Previously, we revealed that FveMYB117a controls leaf morphology and inhibits axillary bud outgrowth by directly regulating the expression levels of *FveYUC4*, *FveIPT2*, *FveCKX1*, and *FveCUC2a* [42, 44]. Notably, *FveMYB117a* and *SL1* exhibit specific and largely overlapping expression in leaflet primordia and marginal protrusions [42-43]. Despite these similar expression patterns, our experimental data demonstrate that FveMYB117a does not directly bind to the *SL1* promoter but instead indirectly activates its transcription (Fig. 2), suggesting that this activation is likely mediated by intermediate transcription factors or other signaling components.

Compared with the respective single mutants, the *fvemyb117a-1 sl1-1* double mutant exhibits a fully simple leaf phenotype, accompanied by a markedly increased leaf shape index, severely compromised leaf expansion, and a pronounced reduction in petiole length. The substantially enhanced phenotypic severity provides compelling evidence that *FveMYB117a* and *SL1* function redundantly and cooperatively to regulate leaf morphological complexity. To gain further mechanistic insights, we performed transcriptomic profiling, which revealed 754 upregulated and 1,192 downregulated genes in the *fvemyb117a-1 sl1-1* relative to the wild type (Fig. 3C-3D). Notably, these differentially expressed genes are significantly enriched in functional categories associated with transcription factors, auxin and cytokinin signaling, suggesting that they constitute a repertoire of potential downstream targets through which *FveMYB117a* and *SL1* coordinately orchestrate leaf development in woodland strawberry.

FveMYB117a and SL1 cooperatively regulate transcription factor expression during leaf morphogenesis

The class I KNOX genes, including *STM*, *KNAT1*, *KNAT2*, and *KNAT6*, are central regulators of leaf complexity [59-62]. In addition, the other two KNOX subfamilies, class II and class M, are thought to play more direct roles in Arabidopsis leaf margin morphogenesis, as both are expressed at the sites of serration initiation within leaf primordia [63-64]. During marginal differentiation, these two classes exert opposing functions: class M genes promote serration formation, whereas class II genes suppress it [63-64]. At the transcriptional level, the CIN-TCP factor TCP5 represses the initiation and outgrowth of leaf serrations through direct activation of *KNAT3* expression [65]. The mutants *fvemyb117a* and *fveult1* exhibit an increased number of leaflets, and RT-qPCR analyses revealed the upregulation of several class I *KNOX* genes [40, 42]. In the present study, we observed that *FveKNAT5La* transcript levels were reduced in the young leaves of all three mutants, with the downregulation in the double mutant *fvemyb117a-1 sl1-*

1 being significantly more pronounced than in either single mutant (Fig. 4C), suggesting a synergistic effect on its repression. Collectively, these results suggest that FveKNOXII may also serve as an important regulatory component in strawberry leaf development, potentially modulating leaf complexity through intricate interactions with class I KNOX members.

The TCP transcription factor family negatively regulates leaf complexity across diverse plant species. In Arabidopsis, simultaneous knockdown of multiple CIN-TCP members converts simple leaves into branched structures generating continuous higher order leaflets, ultimately forming highly complex "super leaves" [66]. In tomato, knockout of *SlTCP24* and *SlTCP29* increases leaflet number and enhances dissection [67], whereas in citrus, loss of *CsTCP2* function leads to increased leaf area [68]. In rose, *RmTCP5* reduces leaf area and alters leaf shape index by repressing *RmYUC5* and *RmCKX5* expression, thereby disrupting auxin and cytokinin homeostasis [69]. In contrast, our study reveals that *FveTCP4* and *FveTCP14* are consistently downregulated in the young leaves of all examined mutants (Fig. 4D and 4E). This expression pattern markedly diverges from the functional profiles of TCP genes reported in the aforementioned species, suggesting that *FveTCP4* and *FveTCP14* may fulfill distinct, and potentially species-specific, regulatory roles in strawberry leaf development.

WOX1 and its orthologs positively regulate leaf expansion in Arabidopsis, soybean and tomato [15–17]. In Arabidopsis, JAG is a transcription inhibitor that controls the development of leaf polarity and regulates the expression of genes controlling lateral organ formation [70]. In woodland strawberry, *FveJAG* is markedly downregulated in *sl1* leaves, implicating it as a potential component of the *SL1* genetic network [43]. Here, we observed that both *FveWOX1* and *FveJAG* were downregulated in young leaves of all three woodland strawberry mutants, with significantly greater reduction in the double mutant than in either single mutant (Fig. 4F and 4G). Based on these results, *FveWOX1* and *FveJAG* are proposed to play a positive role in regulating leaf development in the woodland strawberry.

FveMYB117a and SL1 interact with the auxin and cytokinin pathways

Mutations in auxin metabolism-related genes frequently cause aberrant leaf morphology. In auxin biosynthesis, YUC proteins catalyze the rate-limiting and irreversible conversion of indole-3-pyruvic acid to indole-3-acetic acid (IAA) [71-74]. In strawberry, the *fveyuc4* mutants exhibit narrower leaves with fewer and deeper serrations [75]. Exogenous NAA rescues compound leaf formation in *fvemyb117a* and *sl1*, whereas NPA treatment suppresses trifoliate leaf and serration development [37, 42-43]. In all three mutants, the transcript levels of *FveYUC6* was substantially reduced (Fig. 5B), which correlated with a concurrent significant decrease in the endogenous levels of free IAA and OX-IAA (Fig. 6A and 6B). Collectively, these findings suggest that FveMYB117a and SL1 may impair leaf development by repressing *FveYUC6* transcription, thereby reducing auxin production.

GH3 encodes an auxin amide synthetase that catalyzes the conjugation of auxin to acyl-containing substrates, including amino acids and jasmonic acid, thereby regulating plant growth through auxin homeostasis [76]. Overexpression of *GH3* in rice and citrus reduces free IAA content, leading to auxin-deficient phenotypes such as dwarfism and reduced leaf size [77-78]. In our study, the expression levels

of *FveGH3.2* and *FveGH3.6* were significantly downregulated in all three mutants (Fig. 5C and 5D). Although this repression would theoretically elevate the pool of active IAA in young leaves, our quantitative measurements did not support this prediction (Fig. 6A). This apparent discrepancy between transcriptional changes and phenotypic outcomes suggests a more complex regulatory architecture. Rather than acting directly on the upstream regulatory elements of *FveGH3.2* and *FveGH3.6*, we propose that FveMYB117a and SL1 modulate their expression indirectly through intermediate signaling components or feedback regulatory loops. Consequently, the downregulation of these *GH3* genes may be effectively masked by compensatory mechanisms operating at post-transcriptional or metabolic levels.

As a key enzyme in the cytokinin activation pathway, LOG family proteins are responsible for converting inactive precursors into physiologically active cytokinins, thereby finely regulating plant growth and development [79]. In species like Arabidopsis, tomato, and *Medicago*, cytokinin has been shown to positively regulate developmental events such as leaf primordium initiation, leaf margin serration formation, and leaf expansion [33-35]. In the *fvemyb117a*, the levels of four active cytokinins increased significantly, and exogenous 6-BA treatment noticeably enhanced leaf complexity [42], further supporting the idea that higher cytokinin levels are associated with leaf morphological changes. In this study, we checked the expression of *FveLOG8* in three mutant materials, and all showed downregulated expression (Fig. 5E). Concurrently, we quantified the levels of four cytokinins. These levels were significantly reduced in *sl1-1* and *fvemyb117a-1 sl1-1*, whereas they were significantly increased in *fvemyb117a-1* (Fig. 6C-6F). Considering both the expression and metabolism data, we speculate that in the *fvemyb117a-1*, the downregulation of *FveLOG8* might not be the main factor causing changes in cytokinin levels within the leaves.

Conclusion

In this study, we elucidate the genetic interaction and regulatory gene network between *FveMYB117a* and *SL1* in regulating woodland strawberry leaf morphogenesis. Our findings demonstrate that these two genes function within the same genetic framework, with FveMYB117a indirectly activating *SL1* expression, which leads to a marked reduction in leaf complexity in *fvemyb117a-1 sl1-1*. Transcriptomic profiling consistently reveals the coordinated downregulation of downstream transcription factors-including *FveKNAT5La*, *FveTCP4*, *FveTCP14*, *FveWOX1*, and *FveJAG*-as well as genes involved in auxin (*FveYUC6*, *FveGH3.6*, *FveGH3.2*) and cytokinin (*FveLOG8*) metabolism across all three mutants. Moreover, endogenous hormone measurements in young leaves uncover distinct regulatory divergences: although auxin levels are significantly reduced in all mutants, cytokinin content increases in *fvemyb117a-1* but declines sharply in *sl1-1* and the *fvemyb117a-1 sl1-1*. Collectively, these results provide critical molecular evidence for deciphering the complex regulatory networks governing leaf development in woodland strawberry, thereby laying a theoretical basis for future genetic enhancement and breeding strategies.

Materials and methods

Plant materials and growth conditions

The single mutants *fvemyb117a-1* and *sl1-1* were generated by ethyl methanesulfonate (EMS) mutagenesis at Huazhong Agricultural University in 2016. The double mutant *fvemyb117a-1 sl1-1* was obtained by crossing the single mutants at the Shijiazhuang Fruit Tree Research Institute, Hebei Academy of Agriculture and Forestry Sciences, in 2024. The F_2 population was subsequently genotyped by sequencing. For plant cultivation, seeds were imbibed in water and stratified at 4°C in a refrigerator for approximately 10 days. After germination, they were sown in 15 cm square pots filled with a substrate consisting of vermiculite and peat (1:3, v/v). Woodland strawberry plants were grown in a growth chamber under a photosynthetic photon flux density of 100 μmol m^{-2} s^{-1}, a 16-h light/8-h dark photoperiod, and a constant temperature of 22°C. The primers used for genotyping are listed in Supplementary Table S2.

Leaf morphology analysis

The percentage of leaves with different numbers of leaflets was counted and calculated from mature leaves of WT and mutants of the same age. Select the terminal leaflets from the *fvemyb117a-1* (trifoliate leaves, without obvious lobes), *sl1-1* (simple leaves) and *fvemyb117a-1 sl1-1*, and record leaf length/width, leaf area, and the number of serrations. The distance from the leaf base at the stipule sheath to where the terminal leaflet attaches is considered the petiole length. Mature leaves of WT, *fvemyb117a-1*, *sl1-1*, and *fvemyb117a-1 sl1-1* at the same developmental stage were placed on A4 paper and scanned using an HP Scanjet 8200 scanner to generate silhouettes, making it easier to measure leaf area.

RNA-seq and data analysis

The young leaves (SAM and up to P4 leaves) of *fvemyb117a-1*, *sl1-1*, and *fvemyb117a-1 sl1-1* (30∼40 for each biological replicate) were collected. Sequencing was performed on an Illumina HiSeq 2000 platform (Shanghai Personal Biotechnology Co., Ltd, China). The *F. vesca* reference genome with ver 4.0.a2 annotation was downloaded from the GDR website (https://www.rosaceae.org) [46]. Raw reads were trimmed by 9 bp at the 5' end using Trimmomatic and then mapped to the reference genome using the hisat2 program [48–49]. FeatureCounts was used to count the reads mapped to the gene models [50]. Gene expression levels were calculated as transcripts per million reads (TPM) using Tbtools [51]. Differential gene expression analysis was performed using the R package DESeq2 [52]. Genes with *P*-value < 0.05 and fold change > 1.5, maximum were considered to be differentially expressed. TBtools was used for heatmap generation and KEGG enrichment analysis [51].

RNA extraction and RT-qPCR

Total RNA was extracted using a HiPure Plant RNA Mini Kit (Magen, Guangzhou, China; cat. no. R4151) and reverse-transcribed into cDNA with a PrimeScript™ RT Reagent Kit (TaKaRa, Shiga, Japan; cat. no. RR047A). Quantitative real-time PCR was conducted on a QuantStudio 7 Flex system (Applied Biosystems, Waltham, MA, USA). Relative gene expression levels were calculated via the $2^{-\Delta\Delta CT}$ method,

with FvH4_1g05910 (*FveActin*) serving as the internal reference. Each sample was assayed in three biological replicates (each comprising 10 to 20 tissues), and each biological replicate was subjected to three technical replicates. All primer sequences are provided in Supplementary Table S2.

Yeast one-hybrid assay

The coding sequence of *FveMYB117a* was cloned into the bait vector *p*GADT7, while a 500-bp fragment encompassing the P1 site within the *SL1* promoter was inserted into the *p*AbAi vector. Each recombinant construct, along with the corresponding empty vector, were introduced into the yeast strain Y187. Transformants were plated on TL medium (-Trp/-Leu) and incubated at 30°C for 3–5 days. Upon emergence of single colonies, individual clones were selected for serial dilution, and 100 µL of each dilution was spread onto TLH medium (-Trp/-Leu/-His) supplemented with graded concentrations of 3-aminotriazole (3AT; 0, 1, 5, 10, 20, 30, 50, 70, 100, and 120 mM) and incubated at 30°C for 5–6 days, to assess self-activation and to determine the minimal inhibitory concentration of 3AT. Colonies from control, experimental, and positive-control plates were picked, resuspended in 100 µL of sterile water, and thoroughly mixed. Subsequently, 5 µL of each suspension was spotted onto TL plates and onto TLH plates containing the minimal inhibitory concentration of 3AT, which were then incubated upside down at 30°C for 5–6 days. After sufficient colony growth, the results were recorded. The positive control consisted of *p*HIS2-*p*53 and *p*GADT7-Rec53.

Dual luciferase assay

The full-length coding sequence of *FveMYB117a* was amplified by PCR and fused to GFP in the *p*Cambia1302 vector. The 2.0-kb promoter region of *SL1* was inserted into the *p*GreenII0800 vector to drive the luciferase (LUC) reporter gene. All recombinant constructs and the empty *p*Cambia1302 vector were introduced into *Agrobacterium tumefaciens* strain GV3101 harboring the pSoup19 helper plasmid (WEIDI, Shanghai, China). The effector and reporter cell suspensions were mixed to final OD_{600} values of 0.4 and 0.1, respectively, and infiltrated into *N. benthamiana* leaves. Infiltrations were performed on six independent leaves from separate plants. At 48 h post-infiltration, 1 mM D-luciferin (Solarbio, Beijing, China) was applied to the abaxial leaf surface, and luminescence was captured with a 10 s exposure using a NightSHADE L985 imager. For quantitative measurements, leaf discs were collected and assayed for luciferase (LUC) and Renilla luciferase (REN) activities using the Luciferase Assay System Kit (Promega, USA). Relative firefly luciferase activity was calculated as the LUC/REN ratio for each sample. All primer sequences are provided in Supplementary Table S2.

Electrophoretic mobility shift assay (EMSA)

The coding sequence of *FveMYB117a* was cloned into *p*ET-28a in-frame with a His-tag. The recombinant FveMYB117a-His fusion protein was expressed in *E. coli* Rosetta (DE3) competent cells (WEDI, Shanghai, China) upon induction with 0.5 mM isopropyl β-D-1-thiogalactopyranoside (IPTG; A100487, Sangon Biotech, China) at 37°C for 10 h with shaking. Subsequently, the bacterial cells were harvested, washed, resuspended, and lysed. The His-tagged protein was purified using Ni Smart Beads 6FF (Smart-Lifesciences, China) following the manufacturer's protocol. Wild-type and mutant DNA probes harboring

the cis-elements were commercially synthesized as 5'-biotinylated single-stranded (ss) oligonucleotides (Sangon Biotech, China). Double-stranded (ds) probes were generated by annealing equimolar complementary ss oligonucleotides at 95°C for 2 min, followed by gradual cooling to 25°C at a rate of 0.1°C/s. Unlabeled probes, generated by PCR using the same primer pair, served as specific competitors. For binding assays, the purified protein was incubated with wild-type, mutant, or competing probes in binding buffer (10 mM Tris-HCl, pH 7.5, 50 mM KCl, 1 mM DTT, 2.5% (v/v) glycerol, 5 mM $MgCl_2$, and 0.05% (v/v) NP-40) for 45 min at room temperature. The DNA-protein complexes were resolved on 6% native polyacrylamide gels in 0.5× TBE buffer. The primers used are listed in Supplementary Table S2.

Endogenous auxin and cytokinin quantification

The levels of auxin and cytokinin in the young leaves (SAM and up to P4 leaves) of WT, *fvemyb117a-1*, *sl1-1*, and the *fvemyb117a-1 sl1-1* double mutant were quantified using ultra-performance liquid chromatography coupled with mass spectrometry (UPLC-MS), with three biological replicates per genotype. For each replicate, approximately 100 mg of fresh tissue was harvested, immediately flash-frozen in liquid nitrogen, and subsequently ground into a fine powder. Hormone quantification was performed by MetWare (http://www.metware.cn/) on an AB Sciex QTRAP 6500 LC-MS/MS platform. Briefly, metabolites were extracted from the samples using 1 mL of a methanol/water/formic acid mixture (15:4:1, v/v/v). The extracts were evaporated to dryness under a nitrogen stream, reconstituted in 100 µL of 80% methanol (v/v), and filtered through a 0.22 µm membrane prior to LC-MS analysis. Authentic standards for auxin and cytokinin were obtained from Olchemim Ltd. (Olomouc, Czech Republic) and Sigma-Aldrich (St. Louis, MO, USA). Data acquisition was performed using Analyst 1.6.3 software (AB Sciex), and metabolite quantification was carried out with Multiquant 3.0.3 software (AB Sciex).

Statistical analyses

All statistical analyses were performed using GraphPad Prism 8 software. Pairwise comparisons were conducted via Student's *t*-test (**, $P < 0.01$). Comparisons among multiple groups were assessed using Tukey's test, with significant differences at the $P < 0.05$ level denoted by different letters.

Declarations

Funding

This work was supported by Hebei Province Natural Science Foundation Project (C2025301166), Hebei Academy of Agriculture and Forestry Sciences Technology Innovation Talent Team Building Project (C25R0701 and C26R0702), Hebei Province Modern Agricultural Industry Technology System Apple Innovation Team (HBCT2024150209), Hebei Academy of Agriculture and Forestry Sciences Special Science and Technology Innovation Project (2026KJCXZX-SGS-8) and the Hebei Strawberry Technology Innovation Center (SJ2023052).

Author contributions

CK and YH conceived and designed the experiments; YH performed most of the experiments; YH and CK wrote the manuscript; JF, PL, LL, MY, LY helped interpret the data and revised the manuscript. All the authors have read and approved the paper.

Data availability

The RNA-seq reads have been deposited into CNGB Sequence Archive (CNSA) of China National GeneBank DataBase (CNGBdb) with accession number CNP0010112. The woodland strawberry gene sequences from genome version 4.0 are available through the Genome Database for Rosaceae (http://www.rosaceae.org) with accession numbers: *FveMYB117a*, FvH4_4g31190; *SL1*, FvH4_7g28640.

Ethics approval and consent to participate

Not applicable.

Consent for publication

Not applicable.

Competing interests

The authors declare no competing interests.

References

1. Runions A, Tsiantis M, Prusinkiewicz P. A common developmental program can produce diverse leaf shapes. New Phytol. 2017;216:401–18.
2. Efroni I, Eshed Y, Lifschitz E. Morphogenesis of Simple and Compound Leaves: A Critical Review. Plant Cell. 2010;22:1019–32.
3. Bar M, Ori N. Compound leaf development in model plant species. Curr Opin Plant Biol. 2015;23:61–9.
4. Du F, Guan C, Jiao Y. Molecular Mechanisms of Leaf Morphogenesis. Mol Plant. 2018;11:1117–34.
5. Hareven D, Gutfinger T, Parnis A, Eshed Y, Lifschitz E. The making of a compound leaf: genetic manipulation of leaf architecture in tomato. Cell. 1996;84(5):735–44.
6. Bharathan G, Goliber TE, Moore C, Kessler S, Pham T, Sinha NR. Homologies in leaf form inferred from KNOXI gene expression during development. Science. 2002;296(5574):1858–60.
7. Hay A, Tsiantis M. The genetic basis for differences in leaf form between Arabidopsis thaliana and its wild relative Cardamine hirsuta. Nat Genet 2006:38 (8):942–7.
8. Hay A, Tsiantis M. KNOX genes: versatile regulators of plant development and diversity. Development. 2010;137(19):3153–65.
9. Shani E, Burko Y, Ben-Yaakov L, Berger Y, Amsellem Z, Goldshmidt A, Sharon E, Ori N. Stage-specific regulation of Solanum lycopersicum leaf maturation by class 1 KNOTTED1-LIKE HOMEOBOX

proteins. Plant Cell. 2009;21(10):3078–92.

10. Vlad D, Kierzkowski D, Rast MI, Vuolo F, Dello Ioio R, Galinha C, Gan X, Hajheidari M, Hay A, Smith RS. Leaf Shape Evolution Through Duplication, Regulatory Diversification, and Loss of a Homeobox Gene. Science. 2014;343:780–3.
11. Koyama T, Furutani M, Tasaka M, Ohme-Takagi M. TCP transcription factors control the morphology of shoot lateral organs via negative regulation of the expression of boundary-specific genes in Arabidopsis. Plant Cell. 2007;19:473–84.
12. Koyama T, Mitsuda N, Seki M, Shinozaki K, Ohme-Takagi M. TCP transcription factors regulate the activities of ASYMMETRIC LEAVES1 and miR164, as well as the auxin response, during differentiation of leaves in Arabidopsis. Plant Cell. 2010;22:3574–88.
13. Martín-Trillo M, Cubas P. TCP genes: a family snapshot ten years later. Trends Plant Sci. 2010;15:31–9.
14. Shleizer-Burko S, Burko Y, Ben-Herzel O, Ori N. Dynamic growth program regulated by LANCEOLATE enables flexible leaf patterning. Development. 2011;138:695–704.
15. Zhang Z, Runions A, Mentink RA, Kierzkowski D, Karady M, Hashemi B, Huijser P, Strauss S, Gan X, Ljung K, et al. A WOX/Auxin Biosynthesis Module Controls Growth to Shape Leaf Form. Curr Biol. 2020;30:4857–e48684856.
16. Vandenbussche M, Horstman A, Zethof J, Koes R, Rijpkema AS, Gerats T. Differential Recruitment of WOX Transcription Factors for Lateral Development and Organ Fusion in Petunia and Arabidopsis. Plant Cell. 2009;21:2269–83.
17. Tadege M, Lin H, Bedair M, Berbel A, Wen JQ, Rojas CM, Niu LF, Tang YH, Sumner L, Ratet P, McHale NA, Madueño F, Mysorea KS. STENOFOLIA Regulates Blade Outgrowth and Leaf Vascular Patterning in *Medicago truncatula* and *Nicotiana sylvestris*. Plant Cell. 2011;23:2125–42.
18. Ohno CK, Reddy GV, Heisler MGB, Meyerowitz EM. The Arabidopsis JAGGED gene encodes a zinc finger protein that promotes leaf tissue development. Development. 2004;131:1111–22.
19. David-Schwartz R, Koenig D, Sinha NR. LYRATE Is a Key Regulator of Leaflet Initiation and Lamina Outgrowth in Tomato. Plant Cell. 2009;21:3093–104.
20. Jeong NSS, Kim MH, Lee S, Moon JK, Kim HS, Jeong SC. Ln is a key regulator of leaflet shape and number of seeds per pod in soybean. Plant Cell. 2012;24:4807–18.
21. Wang H, Chen J, Wen J, Tadege M, Li G, Liu Y, Mysore KS, Ratet P, Chen R. Control of Compound Leaf Development by FLORICAULA/LEAFY Ortholog SINGLE LEAFLET1 in Medicago truncatula. Plant Physiol. 2008;146:1759–72.
22. Champagne CEM, Goliber TE, Wojciechowski MF, Mei RW, Townsley BT, Wang K, Paz MM, Geeta R, Sinha NR. Compound Leaf Development and Evolution in the Legumes. Plant Cell. 2007;19:3369–78.
23. Chen J, Yu J, Ge L, Wang H, Berbel A, Liu Y, Chen Y, Li G, Tadege M, Wen J et al. Control of dissected leaf morphology by a Cys(2)His(2) zinc finger transcription factor in the model legume *Medicago truncatula*. Proc. Natl. Acad. Sci. U.S.A. 2010;107: 10754–10759.

24. He L, Liu Y, He H, Liu Y, Qi J, Zhang X, Li Y, Mao Y, Zhou S, Zheng X, et al. A molecular framework underlying the compound leaf pattern of *Medicago truncatula*. Nat Plants. 2020;6:511–21.
25. He L, Liu Y, Mao Y, Wu X, Zheng X, Zhao W, Mo X, Wang R, Wu Q, Wang D, et al. GRAS transcription factor PINNATE-LIKE PENTAFOLIATA2 controls compound leaf morphogenesis in Medicago truncatula. Plant Cell. 2024;36:1755–76.
26. Koenig D, Bayer E, Kang J, Kuhlemeier C, Sinha N. Auxin patterns Solanum lycopersicum leaf morphogenesis. Development. 2009;136(17):2997–3006.
27. Bilsborough GD, Runions A, Barkoulas M, Jenkins HW, Hasson A, Galinha C, Laufs P, Hay A, Prusinkiewicz P, Tsiantis M. Model for the regulation of Arabidopsis thaliana leaf margin development. Proc. Natl. Acad. Sci. U.S.A. 2011;108 (8):3424–3429.
28. Zhao B, He L, Jiang C, Liu Y, He H, Bai Q, Zhou S, Zheng X, Wen J, Mysore KS et al. Lateral Leaflet Suppression 1 (LLS1), encoding the MtYUCCA1 protein, regulates lateral leaflet development in *Medicago truncatula*. New Phytol. 2020;227: 613–628.
29. Barkoulas M, Hay A, Kougioumoutzi E, Tsiantis M. A developmental framework for dissected leaf formation in the Arabidopsis relative *Cardamine hirsuta*. Nat Genet. 2008;40:1136–41.
30. Zhou CHL, Hou C, Metelli A, Qi L, Tadege M, Mysore KS, Wang Z-Y. Developmental Analysis of a Medicago truncatula smooth leaf margin1 Mutant Reveals Context-Dependent Effects on Compound Leaf Development. Plant Cell. 2011;23:2106–24.
31. Wang H, Jones B, Li Z, Frasse P, Delalande C, Regad F, Chaabouni S, Latche A, Pech J-C, Bouzayen M. The Tomato Aux/IAA Transcription Factor IAA9 Is Involved in Fruit Development and Leaf Morphogenesis. Plant Cell. 2005;17:2676–92.
32. Zhang J, Chen R, Xiao J, Qian C, Wang T, Li H, Ouyang B, Ye Z. A single-base deletion mutation in SlIAA9 gene causes tomato (Solanum lycopersicum) entire mutant. J Plant Res. 2007;120:671–8.
33. Shani E, Ben-Gera H, Shleizer-Burko S, Burko Y, Weiss D, Ori N. Cytokinin Regulates Compound Leaf Development in Tomato. Plant Cell. 2010;22:3206–17.
34. Greenboim-Wainberg Y, Maymon I, Borochov R, Alvarez J, Olszewski N, Ori N, Eshed Y, Weiss D. Cross Talk between Gibberellin and Cytokinin: The Arabidopsis GA Response Inhibitor SPINDLY Plays a Positive Role in Cytokinin Signaling. Plant Cell. 2005;17:92–102.
35. Wang X, Zhang J, Chai M, Han L, Cao X, Zhang J, Kong Y, Fu C, Wang ZY, Mysore KS. The role of Class □ KNOX family in controlling compound leaf patterning in *Medicago truncatula*. J Integr Plant Biol. 2023;65:2279–91.
36. Zhang Y, Kan L, Hu S, Liu Z, Kang C. Roles and evolution of four LEAFY homologs in floral patterning and leaf development in woodland strawberry. Plant Physiol. 2023;192:240–55.
37. Luo X, Guo L, Tagliere E, Yang Z, Liu Z. Leaf dissection and margin serration are independently regulated by two regulators converging on the CUC2-auxin module in strawberry. Curr Biol. 2024;34(4):769–e7805.
38. Zheng G, Wei W, Li Y, Kan L, Wang F, Zhang X, Li F, Liu Z, Kang C. Conserved and novel roles of miR164-CUC2 regulatory module in specifying leaf and floral organ morphology in strawberry. New

Phytol. 2019;224:480–92.

39. Wang B, Li W, Xu K, Lei Y, Zhao D, Li X, Zhang J, Zhang Z. A splice site mutation in the *FvePHP* gene is associated with leaf development and flowering time in woodland strawberry. Hortic Res. 2023; 10.
40. Han Y, Kang C. The trithorax group factor ULTRAPETALA1 controls flower and leaf development in woodland strawberry. Plant Sci. 2023;333:111729.
41. Tsiantis M, Chatterjee M, Bermudez-Lozano CL, Clancy MA, Davis TM, Folta KM. A Strawberry KNOX Gene Regulates Leaf, Flower and Meristem Architecture. PLoS ONE. 2011;6.
42. Han Y, Lu R, Yan D, Liu Z, Luo X, Kang C. The transcription factor FveMYB117a controls leaf morphology by coordinating auxin and cytokinin signals in woodland strawberry. Plant Physiol. 2025; 198.
43. Pi M, Zhong R, Hu S, Cai Z, Plunkert M, Zhang W, Liu Z, Kang C. A GT-1 and PKc domain-containing transcription regulator *SIMPLE LEAF1* controls compound leaf development in woodland strawberry. New Phytol. 2022;237:1391–404.
44. Han Y, Qu M, Liu Z, Kang C. Transcription factor FveMYB117a inhibits axillary bud outgrowth by regulating cytokinin homeostasis in woodland strawberry. Plant Cell. 2024;36:2427–46.
45. Prouse MB, Campbell MM. The interaction between MYB proteins and their target DNA binding sites. Biochim Biophys Acta Gene Regul Mech. 2012;1819(1):67–77.
46. Li Y, Pi M, Gao Q, Liu Z, Kang C. Updated annotation of the wild strawberry *Fragaria vesca* V4 genome. Hortic Res. 2019;6.
47. Kamada-Nobusada T, Sakakibara H. Molecular basis for cytokinin biosynthesis. Phytochemistry. 2009;70(4):444–9.
48. Bolger AM, Lohse M, Usadel B. Trimmomatic: a flexible trimmer for illumina sequence data. Bioinformatics. 2014;30(15):2114–20.
49. Kim D, Langmead B, Salzberg SL. HISAT: a fast spliced aligner with low memory requirements. Nat Methods. 2015;12(4):357–60.
50. Liao Y, Smyth GK, Shi W. feature Counts: an efficient general purpose program for assigning sequence reads to genomic features. Bioinformatics. 2014;30(7):923–30.
51. Chen C, Chen H, Zhang Y, Thomas HR, Frank MH, He Y, Xia R. TBtools: an integrative toolkit developed for interactive analyses of big biological data. Mol Plant. 2020;13(8):1194–202.
52. Love MI, Huber W, Anders S. Moderated estimation of fold change and dispersion for RNA-seq data with DESeq2. Genome Biol. 2014;15(12):550.
53. Lee D-K, Geisler M, Springer PS. LATERAL ORGAN FUSION1 and LATERAL ORGAN FUSION2 function in lateral organ separation and axillary meristem formation in Arabidopsis. Development. 2009;136(14):2423–32.
54. Naz AA, Raman S, Martinez CC, Sinha NR, Schmitz G, Theres K. Trifoliate encodes an MYB transcription factor that modulates leaf and shoot architecture in tomato. Proc Natl Acad Sci U S A.

2013;110(6):2401–6.

55. Martinez CC, Li S, Woodhouse MR, Sugimoto K, Sinha NR. Spatial transcriptional signatures define margin morphogenesis along the proximal–distal and medio-lateral axes in tomato (*Solanum lycopersicum*) leaves. Plant Cell. 2021;33(1):44–65.
56. Zhao Y, Liu R, Xu Y, Wang M, Zhang J, Bai M, Han C, Xiang F, Wang ZY, Mysore KS, et al. AGLF provides C-function in floral organ identity through transcriptional regulation of AGAMOUS in *Medicago truncatula*. Proc Natl Acad Sci U S A. 2019;116(11):5176–81.
57. Zhu B, Li H, Hou Y, Zhang P, Xia X, Wang N, Wang H, Mysore KS, Wen J, Pei Y, et al. AGAMOUS AND TERMINAL FLOWER controls floral organ identity and inflorescence development in Medicago truncatula. J Integr Plant Biol. 2019;61(8):917–23.
58. Yang L, Qi S, Touqeer A, Li H, Zhang X, Liu X, Wu S. SlGT11 controls floral organ patterning and floral determinacy in tomato. BMC Plant Biol. 2020;20(1):562.
59. Hake S, Smith HMS, Holtan H, Magnani E, Mele G, Ramirez J. The role of knox genes in plant development. Annu Rev Cell Dev Biol. 2004;20:125–51.
60. Long JA, Moan EI, Medford JI, Barton MK. A member of the KNOTTED class of homeodomain proteins encoded by the STM gene of Arabidopsis. Nature. 1996;379:66–9.
61. Sinha N. Leaf development in angiosperms. Annu Rev Plant Physiol. 1999;50:419–46.
62. Vollbrecht E, Reiser L, Hake S. Shoot meristem size is dependent on inbred background and presence of the maize homeobox gene, knotted1. Development. 2000;127:3161–72.
63. Magnani E, Hake S. KNOX lost the OX: the Arabidopsis KNATM gene defines a novel class of KNOX transcriptional regulators missing the homeodomain. Plant Cell. 2008;20:875–87.
64. Furumizu C, Alvarez JP, Sakakibara K, Bowman JL. Antagonistic roles for KNOX1 and KNOX2 genes in patterning the land plant body plan following an ancient gene duplication. PLoS Genet. 2015;11:e1004980.
65. Yu H, Zhang L, Wang W, Tian P, Wang W, Wang K, Gao Z, Liu S, Zhang Y, Irish VF, Huang T. TCP5 controls leaf margin development by regulating KNOX and BEL-like transcription factors in Arabidopsis. J EXP BOT. 2021;72:1809–21.
66. Challa KR, Rath M, Sharma AN, Bajpai AK, Davuluri S, Acharya KK, Nath U. Active suppression of leaflet emergence as a mechanism of simple leaf development. Nat Plants. 2021;7:1264–75.
67. Hu G, Zhang D, Luo D, Sun W, Zhou R, Hong Z, Munir S, Ye Z, Yang C, Zhang J, et al. SlTCP24 and SlTCP29 synergistically regulate compound leaf development through interacting with SlAS2 and activating transcription of SlCKX2 in tomato. New Phytol. 2023;240:1275–91.
68. Yu Y, Duan Y, Zhao R, Zhang F. A single TCP transcription factor modulates leaf size in Citrus. Hortic. Plant J. 2026;11.
69. Zhu W, Bao Y, Cao H, Li Y, Bao M, Peng T, Zhang W. The TCP transcription factor RmTCP5 shapes leaf development by modulating auxin and cytokinin homeostasis in Rosa multiflora. J Plant Physiol. 2026;320.

70. Wei L, Wen S, Tu Z, Zhao Y, Li H. Overexpression of *Liriodendron tulipifera* JAG Gene (*LtuJAG*) Changes Leaf Shapes in Transgenic *Arabidopsis thalianas*. Int J Mol Sci. 2022;23:1322.
71. Zhao YCS, Fankhauser C, Cashman JR, Cohen JD, Weigel D, Chory J. A role for favin monooxygenase-like enzymes in auxin biosynthesis. Science. 2001;291:306–9.
72. Mashiguchi K, Tanaka K, Sakai T, Sugawara S, Kawaide H, Natsume M, Hanada A, Yaeno T, Shirasu K, Yao H et al. The main auxin biosynthesis pathway in Arabidopsis. Proceedings of the National Academy of Sciences. 2011;108: 18512–18517.
73. Stepanova AN, Yun J, Robles LM, Novak O, He W, Guo H, Ljung K, Alonso JM. The Arabidopsis YUCCA1 Flavin Monooxygenase Functions in the Indole-3-Pyruvic Acid Branch of Auxin Biosynthesis. Plant Cell. 2011;23:3961–73.
74. Won C, Shen X, Mashiguchi K, Zheng Z, Dai X, Cheng Y, Kasahara H, Kamiya Y, Chory J, Zhao Y. Conversion of tryptophan to indole-3-acetic acid by TRYPTOPHAN AMINOTRANSFERASES OF ARABIDOPSIS and YUCCAs in Arabidopsis. Proc. Natl. Acad. Sci. U.S.A. 2011;108: 18518–18523.
75. Lu R, Pi M, Liu Z, Kang C. Auxin biosynthesis gene FveYUC4 is critical for leaf and flower morphogenesis in woodland strawberry. Plant J. 2023;115:1428–42.
76. Bao D, Chang S, Li X, Qi Y. Advances in the study of auxin early response genes: Aux/IAA, GH3, and SAUR. Crop J. 2024;12(4):964–78.
77. Du H, Wu N, Fu J, Wang S, Li X, Xiao J, Xiong L. A GH3 family member, *OsGH3-2*, modulates auxin and abscisic acid levels and differentially affects drought and cold tolerance in rice. J Exp Bot. 2012;63(18):6467–80.
78. Zou X, Long J, Zhao K, Peng A, Chen M, Long Q, He Y, et al. Overexpressing GH3.1 and GH3.1L reduces susceptibility to *Xanthomonas citri subsp. citri* by repressing auxin signaling in citrus (*Citrus sinensis Osbeck*). PLoS ONE. 2019;14(12):e0220017.
79. Kuroha T, Tokunaga H, Kojima M, Ueda N, Ishida T, Nagawa S, Fukuda H, Sugimoto K, Sakakibara H. Functional Analyses of LONELY GUY Cytokinin-Activating Enzymes Reveal the Importance of the Direct Activation Pathway in Arabidopsis. Plant Cell. 2009;21:3152–69.

Figures

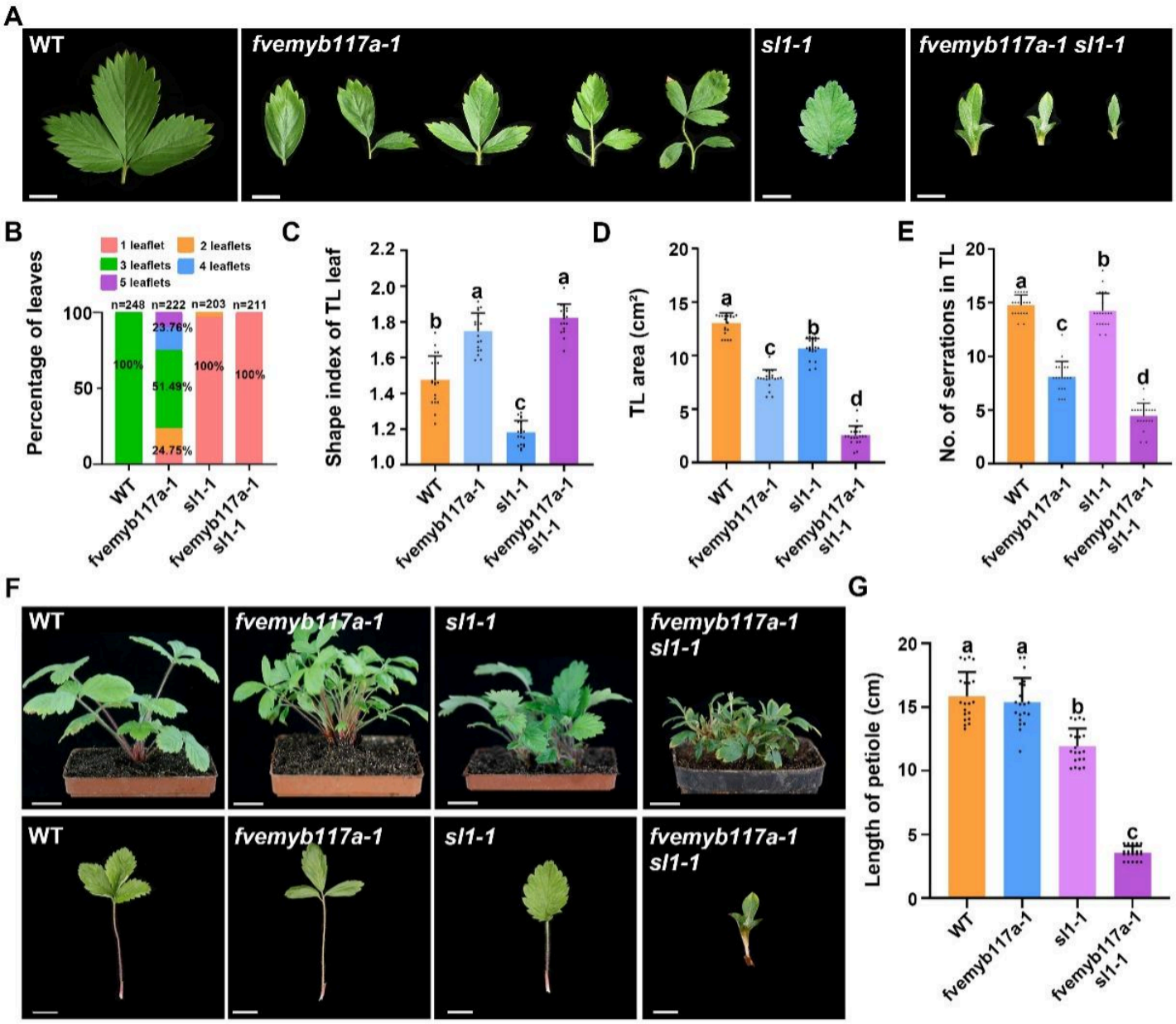


Figure 1

The leaf and petiole morphology of WT, *fvemyb117a-1*, *sl1-1* and *fvemyb117a-1 sl1-1*.

A, Mature leaves of wild type (WT, Ruegen), *fvemyb117a-1*, *sl1-1* and *fvemyb117a-1 sl1-1*. Scale: 0.5 cm. B, Percentage of leaves with 1 to 5 leaflets in WT, *fvemyb117a-1*, *sl1-1* and *fvemyb117a-1 sl1-1*. Numbers 1-5 indicate 1 or 5 leaflets on the petiole. A total of 8-15 samples were counted: n (WT) = 248, n (*fvemyb117a-1*) = 222, n (*sl1-1*) = 203, n (*fvemyb117a-1 sl1-1*) = 211. C-E, The length-to-width ratio, area and number of serrations of terminal leaflets in WT, *fvemyb117a-1*, *sl1-1*and *fvemyb117a-1 sl1-1*. The terminal leaflets without obvious lobing in the C-E were used for statistical analysis. F, The plants and petioles of WT, *fvemyb117a-1*, *sl1-1*, and *fvemyb117a-1 sl1-1*. Scale bars: 5 cm. G, Quantitative analysis of petiole length for each genotype. Data in C-E and G are means ± SD; different letters indicate significant

differences at *P*< 0.05 level determined by Tukey's test. For each genotype, 10 plants were counted, and 2 mature leaves were randomly selected from each plant for measurement, n=20.

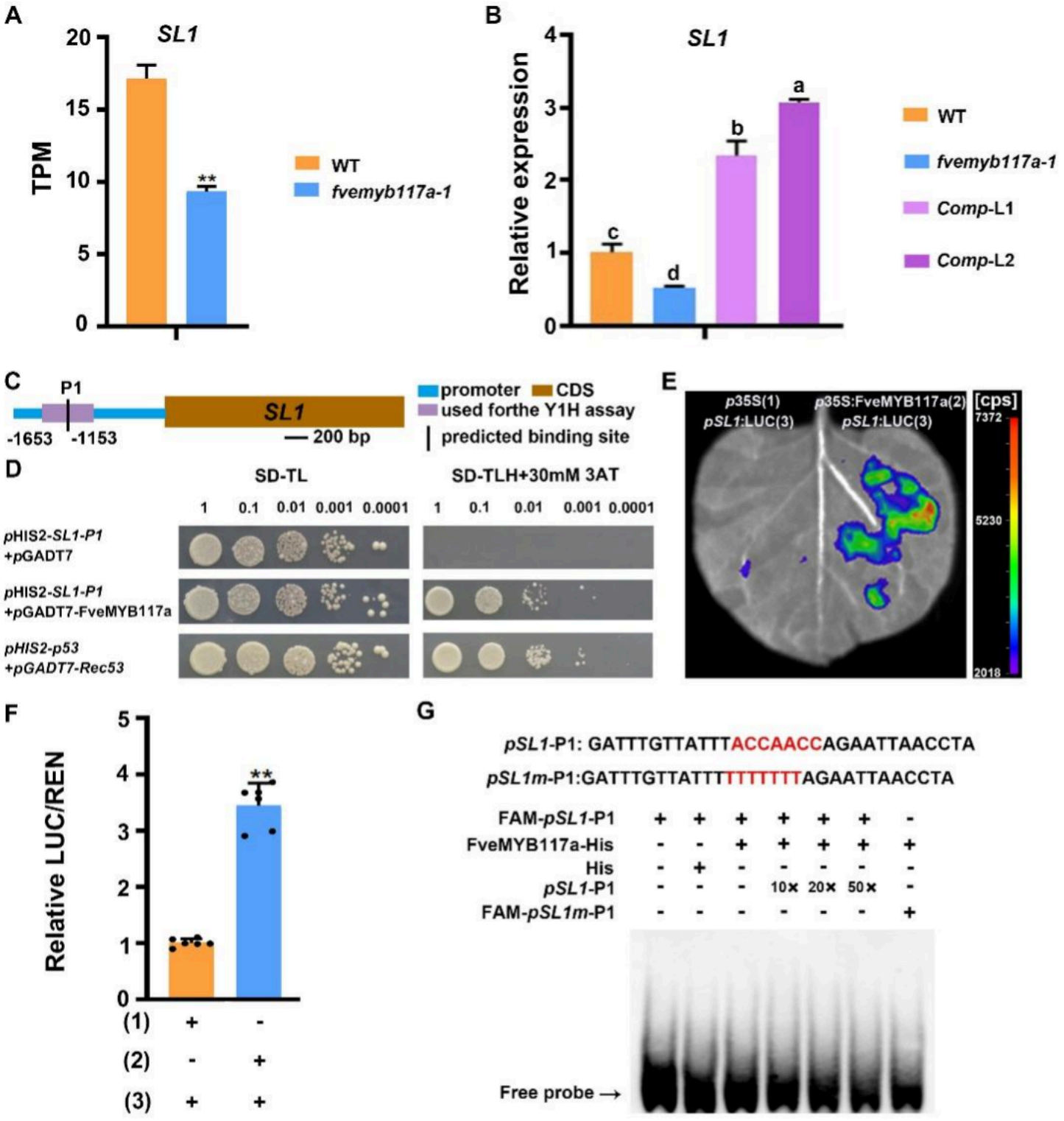


Figure 2

FveMYB117a interacts indirectly with *SL1*during leaf development.

A, TPM values of *SL1* in WT and *fvemyb117a-1* young leaves [42]. B, The expression levels of *SL1*in the young leaves of WT, *fvemyb117a-1* and two complementary lines (P1 to P3) were detected by RT-qPCR. C, Schematic diagram of the gene structure of *SL1*. The dark brown box represents the coding area. The light green box represents the promoter. The black vertical line represents the potential binding element of FveMYB117a. The light purple boxes represent the insertion fragments used for the Y1H experiment. D, The Y1H experiment showed the interaction between FveMYB117a and the *SL1* promoter. Growth of gradient diluted yeast strains on TL and TLH+3AT solid culture media. E, The dual luciferase assay showed the effect of FveMYB117a on the transcriptional activity of the *SL1*promoter. F, The relative LUC activity of the sample in E. G, EMSA experiments show that FveMYB117a can't directly bind to the P1 fragment in the *SL1*promoter. The red letters in oligonucleotides represent the core binding motif. The probe is labeled with FAM. In (A and F), data are the mean± SD of 3 or 6 biological replicates; **, $P< 0.01$; Student's *t*-test. In B, data is the mean ±SD of 3 biological replicates, and significant differences at the $P<0.05$ level are represented by different letters determined by Tukey's test.

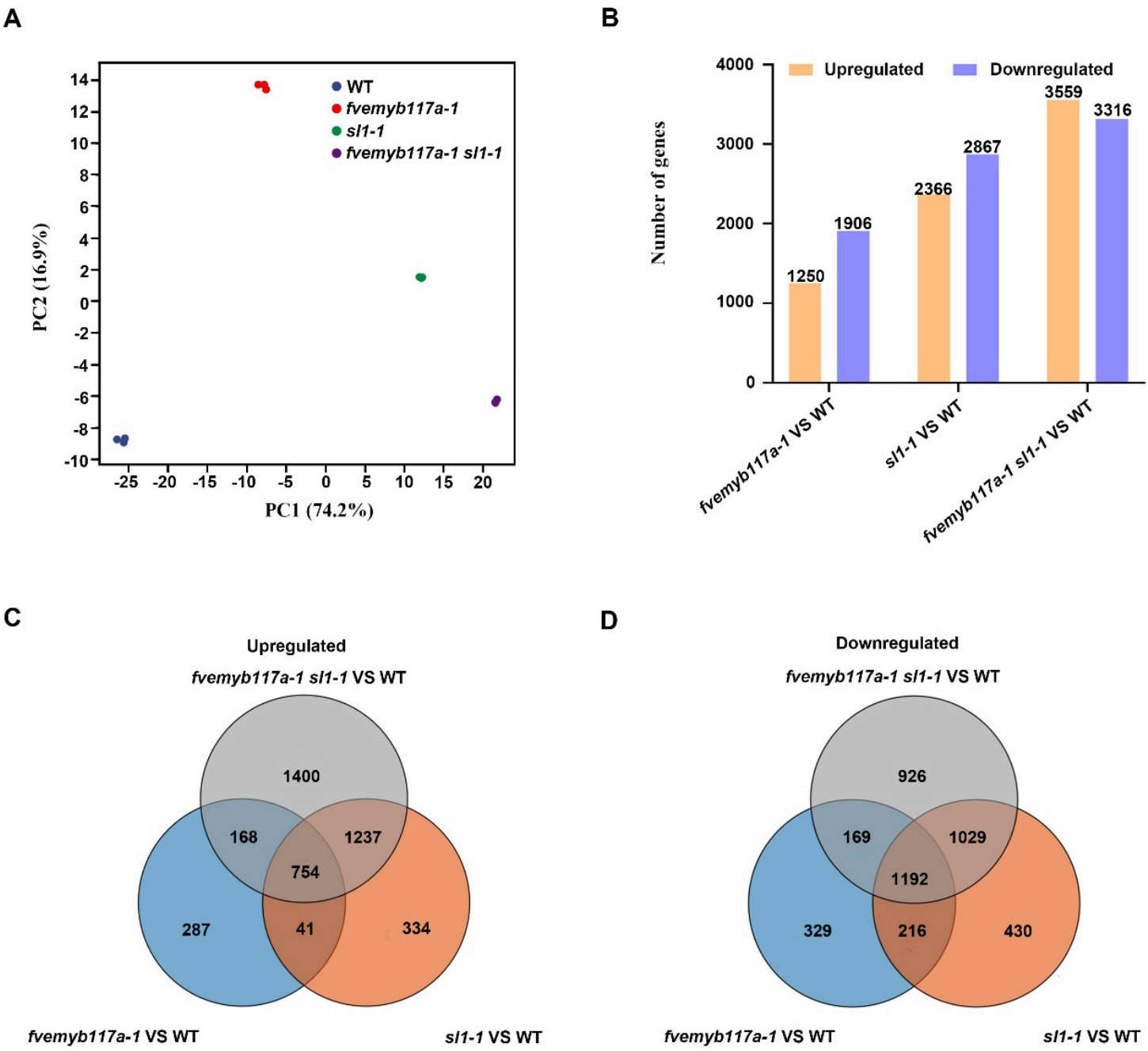


Figure 3

Identification of *FveMYB117a* and *SL1* co-regulated genes by RNA-Seq.

A, PCA analysis of the transcriptome data of young leaves in WT, *fvemyb117a-1*, *sl1-1* and *fvemyb117a-1 sl1-1* (log^2 transformed TPM values of all expressed genes). B, The bar graph shows the number of differentially expressed genes (DEGs) (fold change > 1.5, $P < 0.05$) compared to WT for *fvemyb117a-1*, *sl1-1* and *fvemyb117a-1 sl1-1*. C-D, Venn diagrams show the number of genes that are upregulated or downregulated in common between WT and *fvemyb117a-1*, *sl1-1* and *fvemyb117a-1 sl1-1*.

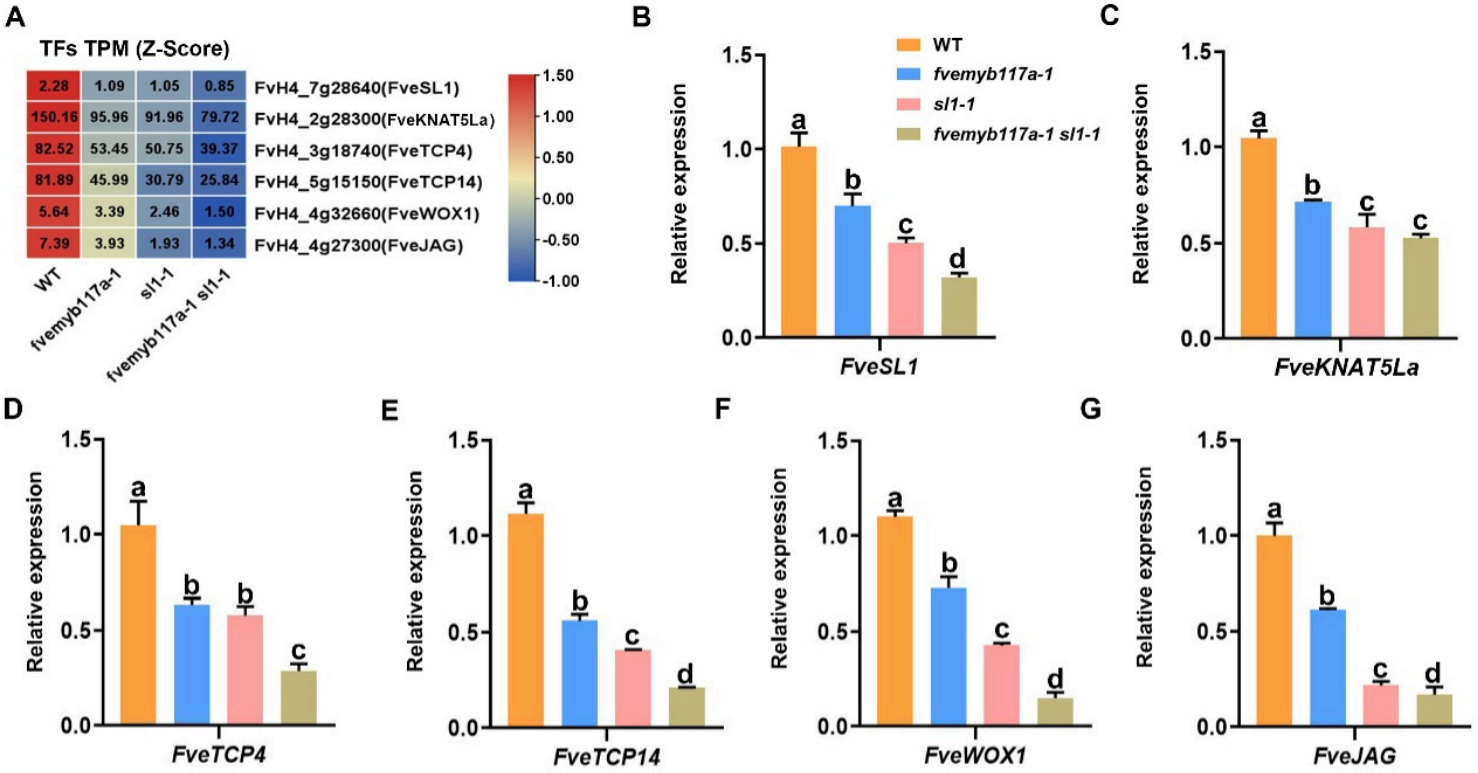


Figure 4

The expression levels of *FveSL1*, *FveKNAT5La*, *FveTCP4*, *FveTCP14*, *FveWOX1* and *FveJAG* in the young leaves of WT and the three mutants.

A, The heatmap shows the expression levels of *FveSL1*, *FveKNAT5La*, *FveTCP4*, *FveTCP14*, *FveWOX1* and *FveJAG* in the young leaves of WT, *fvemyb117a-1*, *sl1-1* and *fvemyb117a-1 sl1-1*. Calculate the average TPM (per million transcripts) value for the 3 biological replicates, and display it in each box. The color represents the Z-score score obtained from the TPM. B-G, RT-qPCR was used to detect the expression levels of *FveSL1*, *FveKNAT5La*, *FveTCP4*, *FveTCP14*, *FveWOX1* and *FveJAG* in the young leaves of WT, *fvemyb117a-1*, *sl1-1* and *fvemyb117a-1 sl1-1*. The data are the average values ± SD of 3 biological replicates, and significant differences at the $P<0.05$ level were determined by the Tukey's test using different letters.

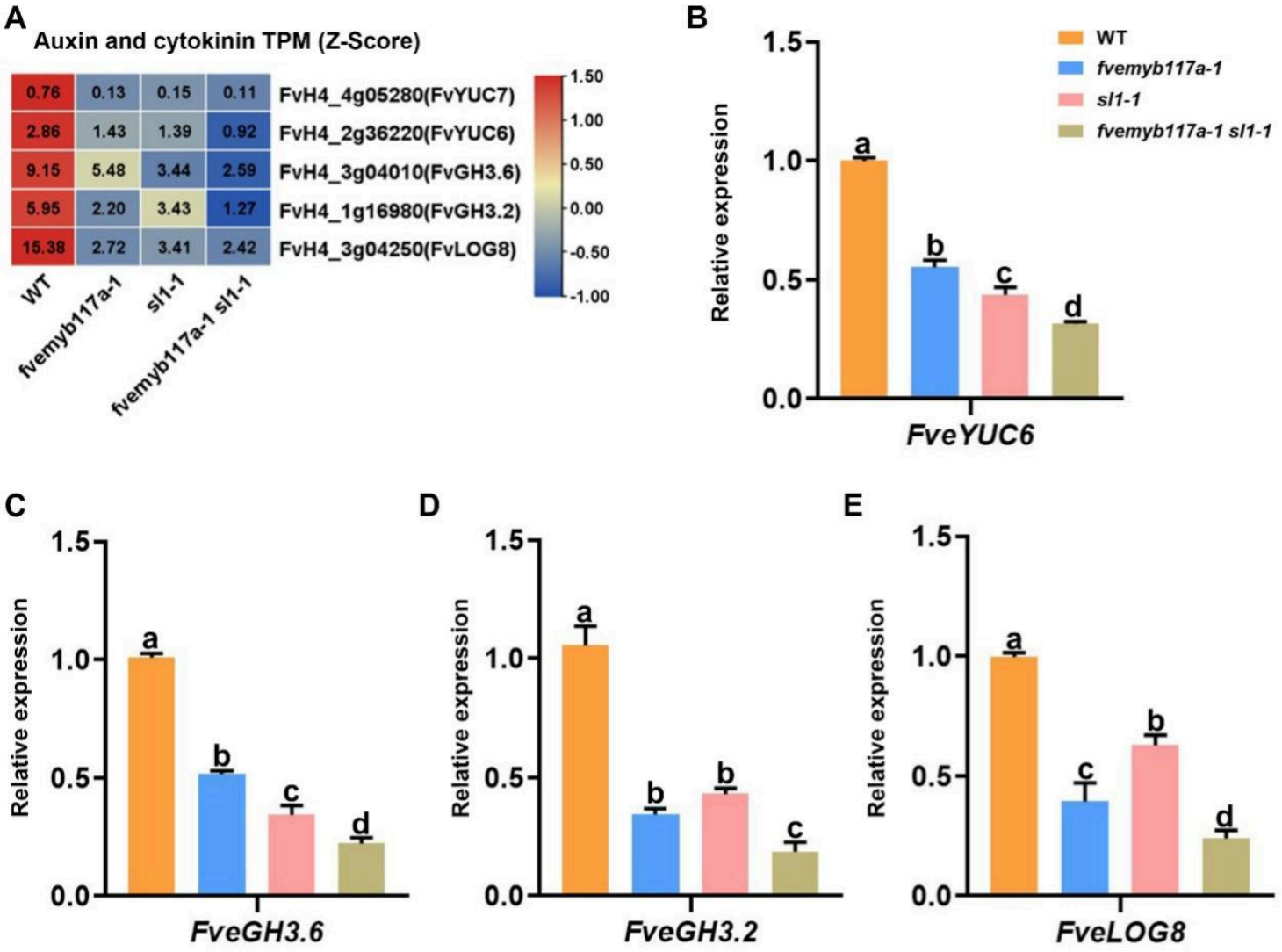


Figure 5

The expression levels of *FveYUC6*, *FveGH3.6*, *FveGH3.2* and*FveLOG8* in the young leaves of WT and the three mutants.

A, The heatmap shows the expression levels of *FveYUC6*, *FveGH3.6*, *FveGH3.2* and *FveLOG8* in the young leaves of WT, *fvemyb117a-1*, *sl1-1* and *fvemyb117a-1 sl1-1*. Calculate the average TPM (per million transcripts) value for the 3 biological replicates, and display it in each box. The color represents the Z-score score obtained from the TPM. B-E, RT-qPCR was used to detect the expression levels of *FveYUC6*, *FveGH3.6*, *FveGH3.2*and *FveLOG8* in the young leaves of WT, *fvemyb117a-1*, *sl1-1* and *fvemyb117a-1 sl1-1*. The data are the average values ± SD of 3 biological replicates, and significant differences at the *P*<0.05 level were determined by the Tukey's test using different letters.

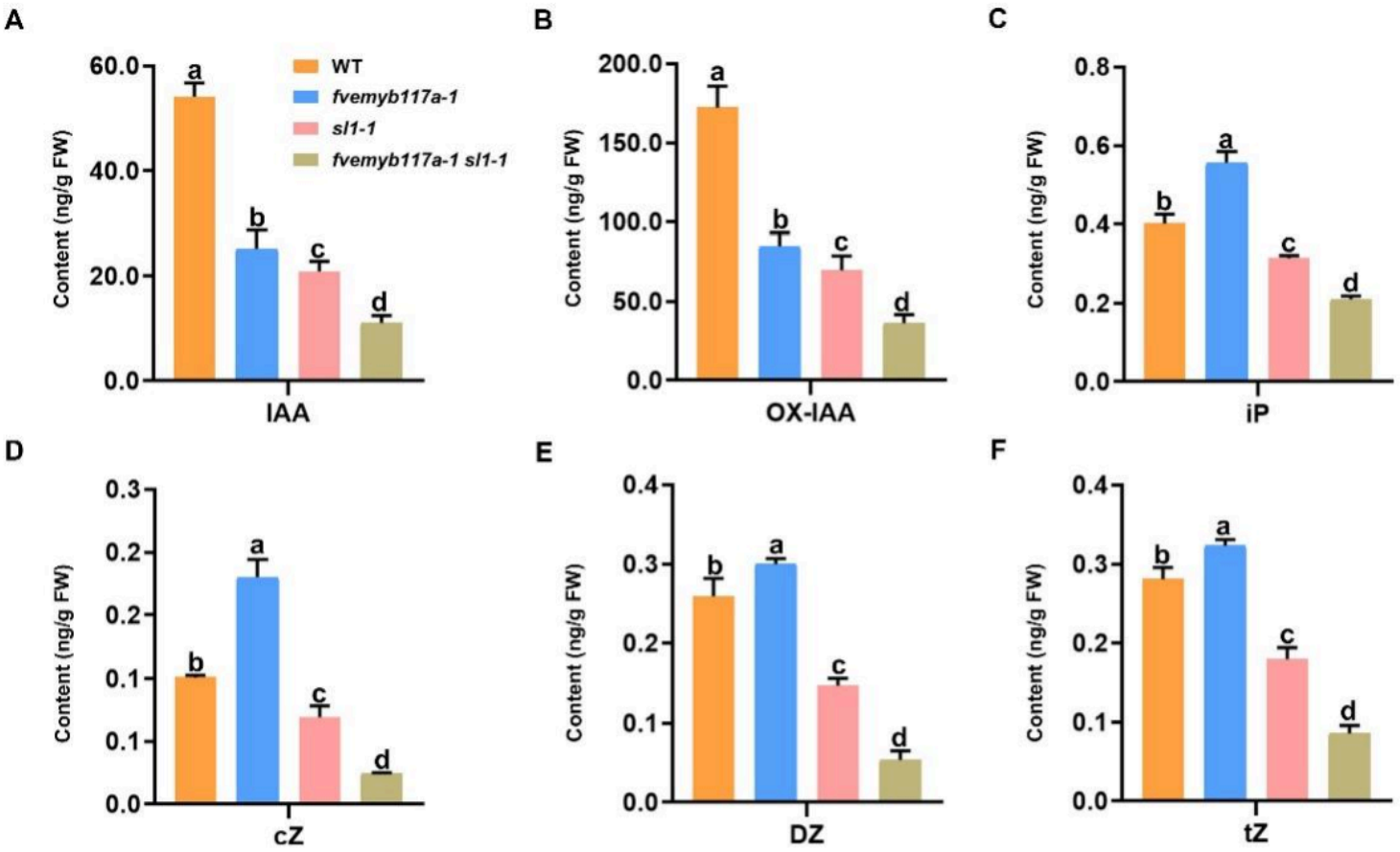


Figure 6

Auxin and cytokinin levels in young leaves of WT, *fvemyb117a-1*, *sl1-1*, and *fvemyb117a-1 sl1-1*.

A-F, The contents of free IAA, OX-IAA and four active cytokinins in the leaves of WT、*fvemyb117a-1*、*sl1-1*and *fvemyb117a-1 sl1-1*. The data in A-F are the average values ± SD of 3 biological replicates, and significant differences at the *P*<0.05 level were determined by the Tukey's test using different letters.

Supplementary Files

This is a list of supplementary files associated with this preprint. Click to download.

- Supplementalfiguresandtables.docx
- DatasetS4.xlsx
- DatasetS5.xlsx
- DatasetS6.xlsx
- DatasetS7.xlsx
- DatasetS1.xlsx
- DatasetS3.xlsx
- DatasetS2.xlsx